

## The fate of land evaporation - A global dataset

Link, Andreas; Van Der Ent, Ruud; Berger, Markus; Eisner, Stephanie; Finkbeiner, Matthias

**DOI**

[10.5194/essd-12-1897-2020](https://doi.org/10.5194/essd-12-1897-2020)

**Publication date**

2020

**Document Version**

Final published version

**Published in**

Earth System Science Data

**Citation (APA)**

Link, A., Van Der Ent, R., Berger, M., Eisner, S., & Finkbeiner, M. (2020). The fate of land evaporation - A global dataset. *Earth System Science Data*, 12(3), 1897-1912. <https://doi.org/10.5194/essd-12-1897-2020>

**Important note**

To cite this publication, please use the final published version (if applicable).  
Please check the document version above.

**Copyright**

Other than for strictly personal use, it is not permitted to download, forward or distribute the text or part of it, without the consent of the author(s) and/or copyright holder(s), unless the work is under an open content license such as Creative Commons.

**Takedown policy**

Please contact us and provide details if you believe this document breaches copyrights.  
We will remove access to the work immediately and investigate your claim.



## The fate of land evaporation – a global dataset

Andreas Link<sup>1</sup>, Ruud van der Ent<sup>2,3</sup>, Markus Berger<sup>1</sup>, Stephanie Eisner<sup>4</sup>, and Matthias Finkbeiner<sup>1</sup>

<sup>1</sup>Chair of Sustainable Engineering, Technical University of Berlin, 10623 Berlin, Germany

<sup>2</sup>Department of Water Management, Faculty of Civil Engineering and Geosciences,  
Delft University of Technology, Delft, the Netherlands

<sup>3</sup>Department of Physical Geography, Faculty of Geosciences, Utrecht University, Utrecht, the Netherlands

<sup>4</sup>Norwegian Institute of Bioeconomy Research, Ås, 1431, Norway

**Correspondence:** Andreas Link (andreas.link@tu-berlin.de)

Received: 16 December 2019 – Discussion started: 27 January 2020

Revised: 17 June 2020 – Accepted: 19 July 2020 – Published: 27 August 2020

**Abstract.** Various studies investigated the fate of evaporation and the origin of precipitation. The more recent studies among them were often carried out with the help of numerical moisture tracking. Many research questions could be answered within this context, such as dependencies of atmospheric moisture transfers between different regions, impacts of land cover changes on the hydrological cycle, sustainability-related questions, and questions regarding the seasonal and interannual variability of precipitation. In order to facilitate future applications, global datasets on the fate of evaporation and the sources of precipitation are needed. Since most studies are on a regional level and focus more on the sources of precipitation, the goal of this study is to provide a readily available global dataset on the fate of evaporation for a fine-meshed grid of source and receptor cells. The dataset was created through a global run of the numerical moisture tracking model Water Accounting Model-2layers (WAM-2layers) and focused on the fate of land evaporation. The tracking was conducted on a  $1.5^\circ \times 1.5^\circ$  grid and was based on reanalysis data from the ERA-Interim database. Climatic input data were incorporated in 3- to 6-hourly time steps and represent the time period from 2001 to 2018. Atmospheric moisture was tracked forward in time and the geographical borders of the model were located at  $\pm 79.5^\circ$  latitude. As a result of the model run, the annual, the monthly and the interannual average fate of evaporation were determined for 8684 land grid cells (all land cells except those located within Greenland and Antarctica) and provided via source–receptor matrices. The gained dataset was complemented via an aggregation to country and basin scales in order to highlight possible usages for areas of interest larger than grid cells. This resulted in data for 265 countries and 8223 basins. Finally, five types of source–receptor matrices for average moisture transfers were chosen to build the core of the dataset: land grid cell to grid cell, country to grid cell, basin to grid cell, country to country, basin to basin. The dataset is, to our knowledge, the first ready-to-download dataset providing the overall fate of evaporation for land cells of a global fine-meshed grid in monthly resolution. At the same time, information on the sources of precipitation can be extracted from it. It could be used for investigations into average annual, seasonal, and interannual sink and source regions of atmospheric moisture from land masses for most of the regions in the world and shows various application possibilities for studying interactions between people and water, such as land cover changes or human water consumption patterns. The dataset is accessible under <https://doi.org/10.1594/PANGAEA.908705> (Link et al., 2019a) and comes along with example scripts for reading and plotting the data.

## 1 Introduction

Where does evaporated water go to, and where is the origin of precipitation? These questions have been addressed by more and more studies within the last few decades, as demonstrated in more detail below. In order to describe the fate of evaporation or the source of precipitation, the concept of atmospheric watersheds was developed in which the terms “evaporationshed” (Van der Ent and Savenije, 2013) and “precipitationshed” (Keys et al., 2012) were introduced. According to Van der Ent (2014), “an evaporationshed describes the downwind atmosphere and surface that receives precipitation from a specific location’s evaporation”, whereas “a precipitationshed is defined as the upwind atmosphere and surface that contributes evaporation to a specific location’s precipitation”.

Several methods are available to identify the origin and fate of moisture, such as analytic box models and physical and numerical (Eulerian and Lagrangian) moisture tracking models (Gimeno et al., 2012). Particularly relevant for large-scale studies are numerical moisture tracking models, which were used in the majority of the more recent studies within this field (Dominguez et al., 2019; Van der Ent et al., 2013; Gimeno et al., 2012). Those models show various application opportunities of which some of the main applications are listed and partly exemplified below:

1. gaining increased knowledge on how regions of interest are dependent on the moisture supply from other regions (Bagley et al., 2012; Dirmeyer et al., 2009; Dominguez et al., 2016; Guo et al., 2019; Keune and Miralles, 2019; Keys et al., 2012, 2018; Salih et al., 2016; Staal et al., 2018; Zhao et al., 2016, 2019),
2. understanding land cover changes and their impacts on the supply of moisture to downwind beneficiaries (Bagley et al., 2012; Keys et al., 2012, 2018; Spracklen et al., 2012; Staal et al., 2018; Tuinenburg et al., 2012; Wang-Erlandsson et al., 2018; Wei et al., 2013, 2016),
3. applications within the context of sustainability and water footprinting (Berger et al., 2014, 2018),
4. understanding the seasonality of precipitation (Guo et al., 2019; Miralles et al., 2016; Zhang et al., 2017) and its interannual variability (Guo et al., 2019; Keys et al., 2018; Sodemann et al., 2008),
5. understanding precipitation changes and trends (Zhang et al., 2017, 2019),
6. investigations into impacts of climate change on the hydrological cycle (Bosilovich et al., 2005; Findell et al., 2019; Singh et al., 2016, 2017),
7. understanding extreme weather events such as droughts and floods (Dirmeyer and Brubaker, 1999; Drumond et

al., 2019; Gangoiti et al., 2011; Gimeno et al., 2016; Herrera-Estrada et al., 2019; Nieto et al., 2019).

The first application refers to moisture supply dependencies for specific regions of interest and practically often comes along with questions related to land cover changes. It can be of importance for regions that mainly rely on rain-fed agriculture where changes in local precipitation could very likely lead to effects on agricultural yields (Van der Ent, 2014; Rockström et al., 2009). Bagley et al. (2012) used results of a numerical moisture tracking in this regard in order to gain knowledge about the sources of precipitation for the major food-producing regions in the world. They analyzed the vulnerability of regions towards a decline in crop productivity while including simulations of alterations in the land cover of surrounding regions (Bagley et al., 2012). Besides regions of rain-fed agriculture, rainforests or urban areas are further regions of interest in research. Staal et al. (2018) investigated, for instance, cascading moisture-recycling effects of the Amazon rainforest, whereas Keys et al. (2018) determined the sources of precipitation and water security challenges for various megacities. Next to investigations into moisture supply dependencies and land cover changes, methods and tools within the context of sustainability are listed as a further potential application possibility. One method which could be named in this context is water footprinting, which quantifies the water consumption and the resulting potential environmental impacts along a product’s life cycle (International Organization for Standardization, 2016). The first considerations for including moisture tracking in water footprinting were accomplished by Berger et al. (2014, 2018). The last application focus exemplified here refers to a deeper understanding of seasonality aspects and the inter-annual variability of precipitation. Guo et al. (2019), for instance, investigated the moisture sources for East Asian precipitation and their temporal variability within this context.

In order to facilitate future applications with regard to atmospheric watersheds, global datasets on the fate of evaporation and the sources of precipitation are needed. However, to our knowledge, only one large-scale approach that tried to track atmospheric moisture globally over a fine-meshed grid exists so far: Dirmeyer et al. (2009) used Lagrangian numerical moisture tracking to determine the sources of precipitation for all land cells across a  $1.9^\circ \times 1.9^\circ$  grid. This resulted in an estimation of the source regions of precipitation for most nations and major basins in the world that has been made publicly available online (DelSole and Dirmeyer, 2012; Dirmeyer et al., 2009).

A comprehensive and global dataset on the fate of land evaporation was so far not readily available to the broader scientific community. Therefore, the goal of this study is to develop a global-scale dataset on the fate of land evaporation for a fine-meshed grid of source and receptor cells that is openly available in a long-term data repository. The results of the study will be presented as source–receptor matri-

ces depicting the yearly average moisture transfers between grid cells. Besides yearly averages, the dataset will comprise monthly averages and data in interannual resolution. The dataset should enable researchers to gain comprehensive information on the fate of evaporation for any land area of interest covered by the model. Additionally, the goal is to provide information about source–receptor matrices for land areas of a high potential interest such as countries or basins.

## 2 Material and methods

We used the Eulerian numerical moisture tracking model Water Accounting Model-2layers (WAM-2layers) to create the dataset, which is able to spatially track tagged moisture forward and backward in time – on regional and global scales (Van der Ent, 2014). The WAM-2layers method and its predecessor version have been used extensively (e.g., in Van der Ent and Savenije, 2013; Findell et al., 2019; Guo et al., 2019; Keys et al., 2012, 2018; Keys and Wang-Erlandsson, 2018; Wang-Erlandsson et al., 2018; Zemp et al., 2017; Zhang et al., 2017, 2019; Zhao et al., 2016) and showed results that were consistent with studies using other tracking methods (Van der Ent et al., 2013). We applied the Python version of the model, which is available on GitHub (Van der Ent, 2019), and modified preprocessing and post-processing. The atmospheric moisture tracking was conducted forward in time, thus focusing on the fate of evaporation. The considered grid covered the globe from 79.5° N to 79.5° S latitude. Calculations were performed on a 1.5° latitude  $\times$  1.5° longitude grid, leading to a total amount of 25 680 grid cells (107  $\times$  240). In order to reduce the computational costs, the amount of cells for which the tracking has been applied was reduced to cells which contain land masses or are located within bigger inland lakes (e.g., the Caspian Sea). The land masses of Greenland and Antarctica were excluded because Eulerian moisture tracking at high latitudes is prone to errors due to high wind speeds compared to the size of the grid cell. As a result, 8684 cells were targeted for the atmospheric moisture tracking. The exact geographical information on the grid and the cells considered for tracking were summarized and are part of the provided dataset.

ERA-Interim (ERA-I) reanalysis data were used as input for the model, which are provided by the European Centre for Medium Range Weather Forecasting (ECMWF) (Berrisford et al., 2011; Dee et al., 2011). The considered time horizon for the input data refers to the period of 2000 to 2018. However, the results are going to be presented for the period of 2001 to 2018, as the first year was used as a model spin-up. The following data items were used as input parameters for the model:

- evaporation and precipitation;
- wind components in zonal and meridional directions;
- specific humidity;

- surface pressure;
- total column water and total column water vapor;
- vertical integral of eastward water vapor flux, vertical integral of eastward cloud liquid water flux, and vertical integral of eastward cloud frozen water flux;
- vertical integral of northward water vapor flux, vertical integral of northward cloud liquid water flux, and vertical integral of northward cloud frozen water flux.

Evaporation and precipitation inputs were incorporated on a 3-hourly basis. All other data items were integrated into the model on a 6-hourly basis. The download of the data occurred at model levels spanning the atmosphere from zero pressure to surface pressure, which are broken down by the model to two layers with well-mixed conditions. The point of division depends on the surface pressure (Van der Ent et al., 2014, Eq. B5) but is at approximately 2 km height for a standard surface pressure of 101 325 Pa. This division was found to best represent sheared wind systems with wind in the bottom layer going in different direction to wind in the top layer and is most relevant within the tropics where wind shears are particularly strong and a single-layer assumption would be too fault-prone (Van der Ent et al., 2013, Fig. 11; Goessling and Reick, 2013, Fig. 3).

The underlying principle of the WAM-2layers model is the water balance shown in Eq. (1), which was applied in a replicate manner for each time step across the entire grid:

$$\frac{\partial S_k}{\partial t} + \frac{\partial(S_k u)}{\partial x} + \frac{\partial(S_k v)}{\partial y} = E_k - P_k + \xi_k \pm F_v, \quad (1)$$

$S_k$  represents the atmospheric moisture storage in layer  $k$ , and  $t$  stands for time. The subscript  $k$  stands either for the top or the bottom layer. The variables  $u$  and  $v$  are describing the wind directions in zonal ( $x$ ) and meridional ( $y$ ) directions and represent the horizontal moisture transport between grid cells. Evaporation entering a layer is described by  $E_k$ , and precipitation removed from a layer is described by  $P_k$ .  $\xi_k$  is a residual, which is a result of data assimilation in ERA-I and different spatial and temporal resolutions in the calculation steps of the WAM-2layers model. The last term of the equation ( $F_v$ ) describes the vertical moisture transport between the two layers. This term is the one that is most difficult to calculate due to dispersive moisture exchange, aside from transport by average vertical wind speeds (Dominguez et al., 2019). In WAM-2layers it is assumed to be the closure term of the water balance. However, complete closure is not always possible and the net vertical flux was determined such that the water balance error is moisture-weighted equally for both layers. The gross vertical flux is parameterized to be 4 times the net flux in the direction of the net flux and 3 times the net flux in the opposite direction. More detailed information on the determination of all single terms from Eq. (1) is given in the work of Van der Ent et al. (2014, Appendix B).

**Table 1.** Exemplary source–receptor (evaporation–precipitation) matrix – source cells refer to considered land cells only, whereas receptor cells cover all grid cells between 79.5° N and 79.5° S latitude.

Source–receptor matrix	Source cell 1	Source cell 2	...	Source cell 8684
Receptor cell 1	...	...	...	...
Receptor cell 2	...	...	...	...
...	...	...	...	...
Receptor cell 25 680	...	...	...	...

The main calculations were conducted on the massively parallel computing system of the North-German Supercomputing Alliance (HLRN). During the first post-processing, the results were then aggregated to 13 source–receptor matrices with  $8684 \times 25\,680$  cells: 12 for the monthly averages and 1 for the yearly average moisture transfers of the considered time period. Besides the yearly and monthly averages, matrices were also compiled on an interannual basis. Table 1 exemplifies the general structure of a source–receptor matrix. The source cells refer within this context to land cells only, whereas the receptor cells cover the whole considered grid.

Using Eq. (2), we verified in each case how well the water balance closes:

$$\Delta_{\text{closure}} = (E_{\text{input}} - E_{\text{assigned}} - L_{\text{north}} - L_{\text{south}} - L_{\text{system}}) / (E_{\text{input}}), \quad (2)$$

where  $\Delta_{\text{closure}}$  represents the mismatch within the water balance,  $E_{\text{input}}$  is the amount of evaporation input,  $E_{\text{assigned}}$  is water tracked over the considered grid until the point of re-precipitation,  $L_{\text{north}}$  and  $L_{\text{south}}$  are unassigned fractions of tracked water that got lost via the system boundaries (latitudes higher than 79.5° N/S), and  $L_{\text{system}}$  are system losses. The latter term describes unassigned water that is “lost” from the system in the rare case the tracked water would exceed the total water. It may occur especially over mountainous areas or during heavy rainfall, whereby the simplified offline tracking does not correspond to the more advanced weather model of ERA-I, or it may be caused by imbalances due to data assimilation in ERA-I. Mismatches within the water balance could occur because we tracked moisture for all months simultaneously while using the simplified assumption that the water supply from month  $N - x$  to month  $N$  will approximately be the same as from month  $N$  to month  $N + x$ . However, the reality might certainly be characterized in addition by cross-period moisture transfers.

In order to also develop source–receptor matrices for larger regions of interest, moisture transfers of grid cells located within basins or countries were aggregated. Grid cells which contributed only partly to a basin or country were allocated according to the extent of overlap with the respective target area. The described procedure was done with the help of the ArcGIS software in which firstly a country and secondly a basin layer were overlain with the  $1.5^\circ \times 1.5^\circ$  grid. With regard to countries, the global country bound-

aries from DIVA-GIS with 265 countries were used, which were provided on the ArcGIS website (Cun, 2016). We highlight that we do not have any political intentions by referring to this list and that we used it merely as a means of exemplification. Regarding the basins, the basin mask from the WaterGAP3 model (Eisner, 2016) was applied for the overlaying. Due to geographical boundaries at 79.5° latitude N/S, 8223 basins were considered in total. After the overlaying of the respective maps, the geometric intersections were determined within ArcGIS. This was followed by a post-processing in Python dedicated to the creation of the final source–receptor matrices for countries and basins. Finally, the following five types of source–receptor matrices for average moisture transfers were chosen to build the core of the dataset: land grid cell to grid cell, country to grid cell, basin to grid cell, country to country and basin to basin. With regard to the latter two matrices, the quantification of moisture contributions to and from the sea was targeted in addition to moisture transfers between countries and basins, respectively. This was achieved as follows.

- A country’s or basin’s share of precipitation originating from the sea was calculated via the difference in total precipitation and the sum of precipitated water originating from countries (or basins).
- A country’s or basin’s total amount of evaporated water that reprecipitates over the sea was calculated via the difference between the reprecipitation over the whole grid and the one taking place over the sum of countries (or the sum of basins).

Finally, usage possibilities of the created dataset were shown via site-specific examples. Examples were chosen with the objective to cover at least all continents and a wide variety of climate zones.

## 3 Results

### 3.1 Source–receptor matrices

The gained source–receptor matrices represent the main results of the created dataset. Table 2 specifies the different matrix types, the allocation of source and receptor regions to columns and rows, and the numbers of matrices.

**Table 2.** Source–receptor matrices of the created dataset (type 1: land grid cell to grid cell; type 2: country to grid cell; type 3: basin to grid cell; type 4: country to country; type 5: basin to basin).

Type	From (source) – matrix columns	To (receptor) – matrix rows	Number of matrices
1	8684 land grid cells	25 680 grid cells	13 (monthly + yearly averages) + 18 × 13 (separate interannual data for the years 2001 to 2018)
2	265 countries	25 680 grid cells	13 (monthly + yearly averages)
3	8223 basins	25 680 grid cells	13 (monthly + yearly averages)
4	265 countries + sea	265 countries + sea + unassigned	13 (monthly + yearly averages)
5	8223 basins + sea	8223 basins + sea + unassigned	13 (monthly + yearly averages)

Particularly important is the provision of type 1 matrices within the dataset, as they represent the raw data on a grid cell basis from which any further aggregation to larger land areas of interest could potentially take place. Together with the type 2 (country to grid) and type 3 (basin to grid) matrices, they enable the plotting of evaporationsheds over the whole area of the considered grid. The matrices of type 4 and 5, on the other hand, allow for the generation of self-explanatory source–receptor tables between countries and basins, respectively.

Besides the relevant source–receptor matrices, mismatches within the water balance ( $\Delta_{\text{closure}}$ ), as well as all other terms of Eq. (2), are provided within the dataset. Identified mismatches are in general negligibly small for the annual averages (on average 0.03 % for land grid cells) but reach higher values on a monthly basis (on average 12.6 % for land grid cells). Unassigned fractions of moisture were exclusively allocated to losses via the northern and southern boundaries of the model. Thus, system losses due to storage limits play no role at all.

### 3.2 Visualization of sample evaporationsheds

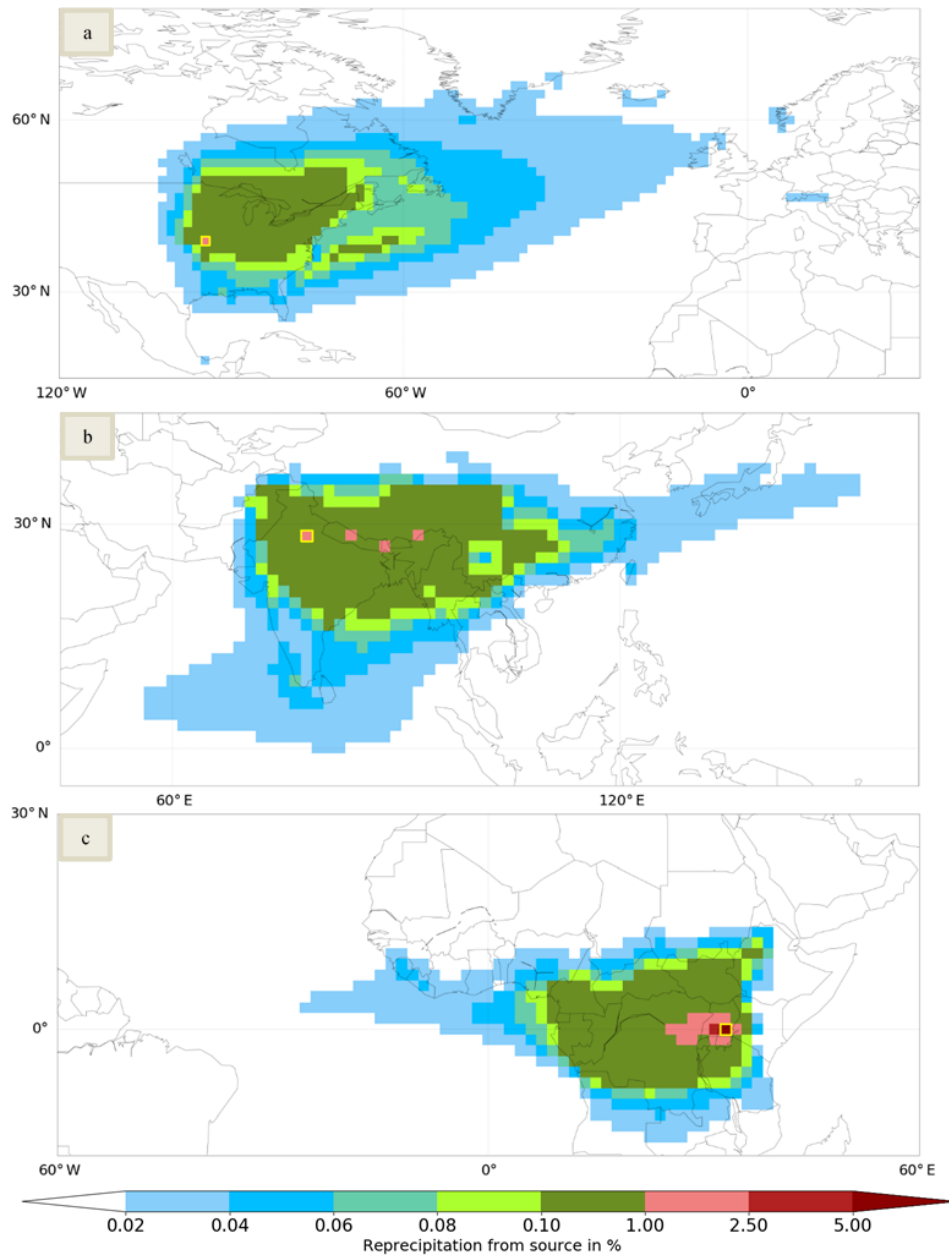
Figures 1 to 3 display the yearly average evaporationsheds for three chosen land grid cells, countries and basins. Based on sample scripts provided within the dataset, these types of figures can be plotted for any land grid cell, country or basin of interest. An additional online viewer can be used to directly look up the plots for any land grid cell. Reprecipitation of evaporated water takes place over the whole considered grid and is expressed as a percentage of the evaporated water from the source region. The threshold for the plotting of reprecipitation within different grid cells lies at 0.02 % from the total amount of the assigned water. Additional information with regard to the location, the total evaporation input into the system ( $E_{\text{input}}$ ), the unassigned fractions of water and the total share of reprecipitation displayed via the plot are provided separately via the image captions. Monthly information on moisture transfers for the chosen examples are available within the Supplement (Figs. S1 to S36).

Figure 1 shows the evaporationsheds for land grid cells located at Kansas City, USA (Fig. 1a), Delhi, India (Fig. 1b), and Kampala, Uganda (Fig. 1c). It exemplifies different pos-

sible shapes and geographical extents of evaporationsheds. The evaporationshed for the source cell at Kansas City sprawls, for instance, over large distances and still does not cover more than 70.0 % of the assigned reprecipitation. The evaporationsheds for the source cells at Kampala and Delhi, on the other hand, cover considerably higher shares of the assigned reprecipitation (79.0 % for Fig. 1b and 88.8 % for Fig. 1c). With regard to the source cell at Kampala, huge amounts of moisture reprecipitate close to the source of evaporation and, thereof, more than 5 % within the source cell itself. Reprecipitation of evaporated water occurs here mainly westwards from the source cell along the equatorial belt and covers huge areas of central Africa. For the other source cells, moisture recycling takes place mainly eastwards (Kansas City) and southeastwards (Delhi) with lower shares of reprecipitation close to the source of evaporation. The tracking of atmospheric moisture for the source cell at Kansas City led to slight boundary losses due to its location near the northern boundary of the model. With regard to Delhi and Kampala, unassigned fractions of moisture due to losses of tagged moisture via the northern or southern boundaries are negligible.

Figure 2 displays evaporationsheds for the example countries Brazil (Fig. 2a), Egypt (Fig. 2b) and Laos (Fig. 2c). Brazil shows a non-fragmented evaporationshed with a huge amount of moisture recycling occurring within the country itself. Egypt's evaporationshed is fragmented, with moisture recycling taking place close to the equatorial belt, over the Mediterranean, and in the southeast of Europe and Asia. However, hardly any reprecipitation occurs within the country. The evaporationshed of Laos is again non-fragmented, with the main areas of moisture recycling in Southeast Asia, over the surrounding sea or in China.

Figure 3 presents the example evaporationsheds for basins referring to parts of the Rio Grande (Fig. 3a), the Danube (Fig. 3b) and the Murray–Darling (Fig. 3c) basin. Core areas of moisture recycling are Central and North America (Fig. 3a), the equatorial belt and huge parts of Eurasia (Fig. 3b), and northern and eastern Australia and the South Pacific Ocean (Fig. 3c). Displayed evaporationsheds are large while covering only 59.4 % to 70.1 % of the assigned moisture recycling.



**Figure 1.** Examples for yearly evaporationsheds of grid cells. **(a)** Cell at 39.0° N latitude and 94.5° W longitude (Kansas City, US;  $E_{\text{input}}$ : 871.6 mm a<sup>-1</sup>; unassigned: 2.3 %); the colored area covers 70.0 % of the assigned water. **(b)** Cell at 28.5° N latitude and 78.0° E longitude (Delhi, India;  $E_{\text{input}}$ : 1132.7 mm a<sup>-1</sup>; unassigned: 0.1 %); the colored area covers 79.0 % of the assigned water. **(c)** Cell at 0.0° latitude and 33.0° E longitude (Kampala, Uganda;  $E_{\text{input}}$ : 1145.1 mm a<sup>-1</sup>; unassigned: 0.0 %); the colored area covers 88.8 % of the assigned water.

### 3.3 Examples for source–receptor tables

Besides the visualization of evaporationsheds, the dataset enables a direct quantification of average moisture transfers between countries or basins within source–receptor tables. This aspect refers to the latter two matrix types (type 4 and 5). At this point, type 4 matrices (countries) are used to demonstrate the usage of both types of matrices. Table 3 shows the fate of evaporated water and the sources of precipitation for

the selected countries. For comparative purposes, the same countries are displayed as for the plotting examples in Fig. 2. The presented information is in each case limited to the top 10 sites of reprecipitation and the top 10 sources of precipitation. Values are provided in percent and are related to the total amount of the evaporation or the precipitation input.

The presented shares with regard to the fate of evaporation are in line with the visualization of evaporationsheds

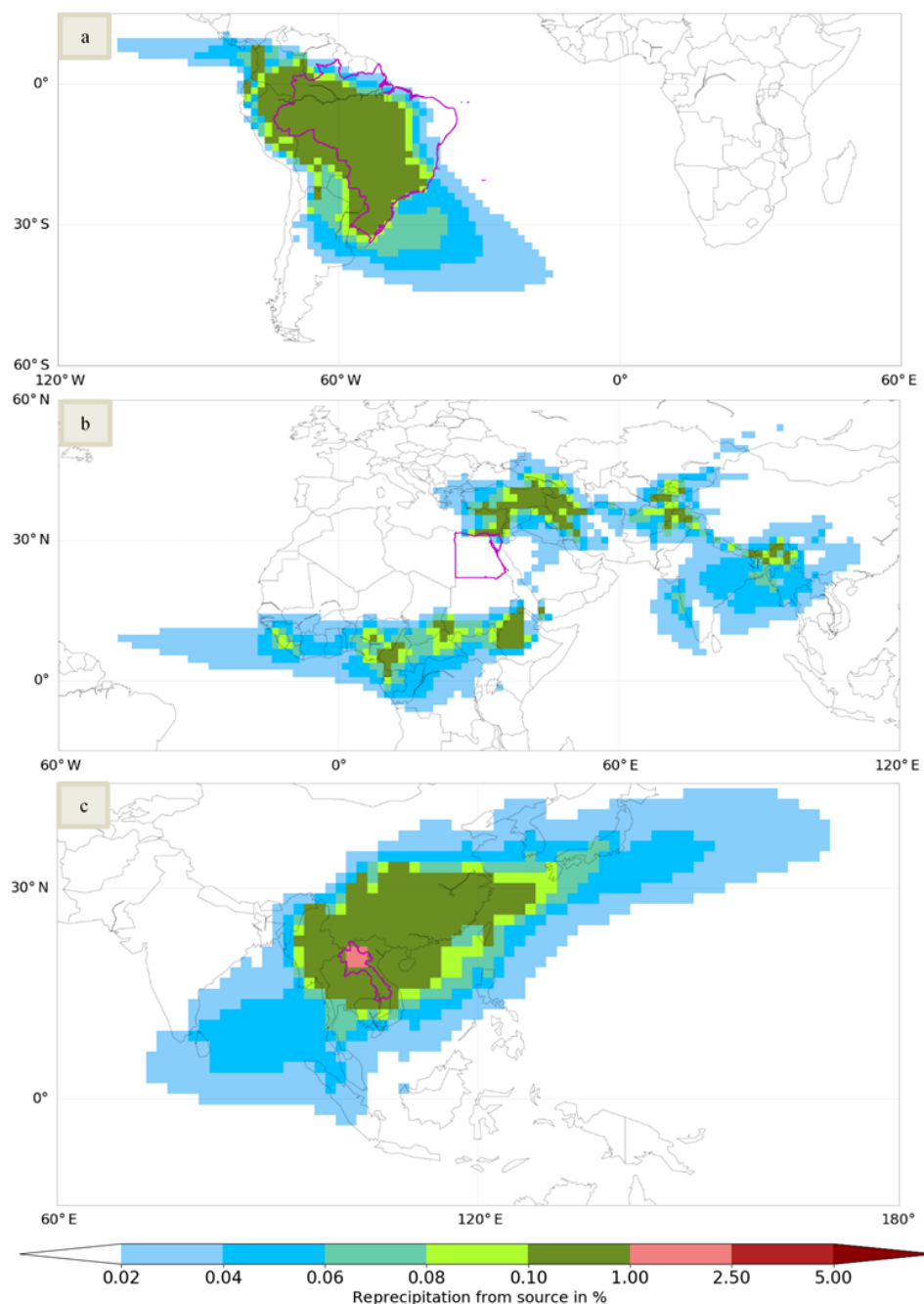


**Figure 2.** Examples for yearly evaporationsheds of countries. **(a)** Brazil ( $E_{\text{input}}$ :  $1240.2 \text{ mm a}^{-1}$ ; unassigned: 0.1 %): the colored area covers 80.4 % of the assigned water. **(b)** Egypt ( $E_{\text{input}}$ :  $104.0 \text{ mm a}^{-1}$ ; unassigned: 0.8 %): the colored area covers 59.9 % of the assigned water. **(c)** Laos ( $E_{\text{input}}$ :  $1178.9 \text{ mm a}^{-1}$ ; unassigned: 0.4 %): the colored area covers 77.9 % of the assigned water.

in Fig. 2. For Brazil, the highest share of reprecipitation takes place within the country (43.6 %). With regard to Egypt and Laos, the highest share of evaporated water reprecipitates over the sea (Egypt: 31.3 %; Laos: 44.5 %). Concerning additional information on the origin of precipitation, Table 3 highlights the following: in all cases the sea is the biggest source of precipitation with values ranging from

63.3 % (Brazil) to 76.6 % (Egypt). With regard to Brazil and Egypt, the most important terrestrial source of precipitation is the country itself (Brazil: 28.9 %, Egypt: 2.7 %). The most relevant terrestrial evaporative source for the precipitation in Laos is Thailand, which supplies on average 6.4 % of the local precipitation.



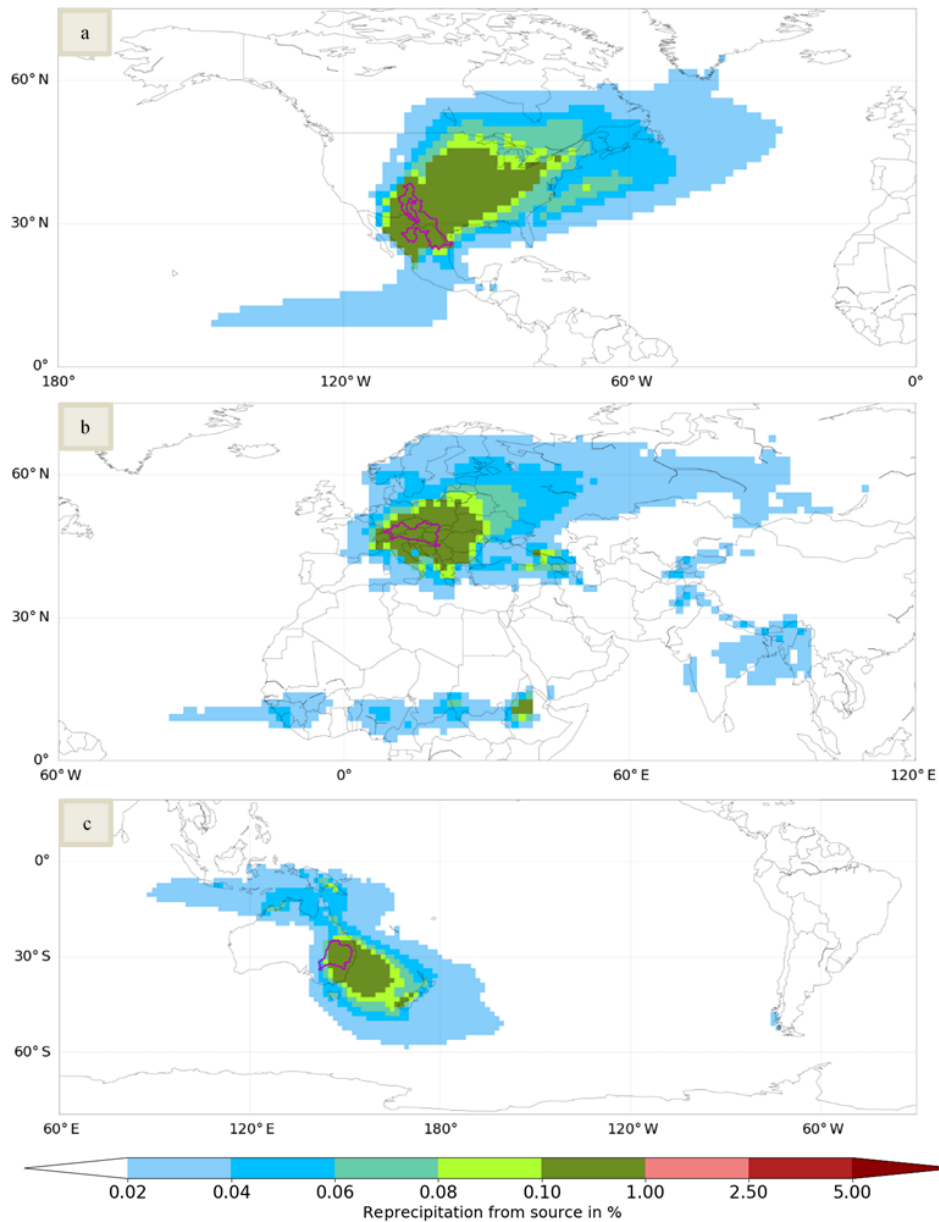


**Figure 3.** Examples for yearly evaporationsheds of basins. **(a)** Basin ID 1463188 (part of the Rio Grande basin;  $E_{\text{input}}$ :  $502.4 \text{ mm a}^{-1}$ ; unassigned: 1.3 %): the colored area covers 70.1 % of the assigned water. **(b)** Basin ID 1019324 (part of the Danube basin;  $E_{\text{input}}$ :  $609.4 \text{ mm a}^{-1}$ ; unassigned: 4.0 %): the colored area covers 60.6 % of the assigned water. **(c)** Basin ID 2245569 (part of the Murray–Darling basin;  $E_{\text{input}}$ :  $503.5 \text{ mm a}^{-1}$ ; unassigned: 0.5 %): the colored area covers 59.4 % of the assigned water.

## 4 Discussion

### 4.1 Possible uses of the dataset

The introduction already provided a broad overview on various uses of numerical moisture tracking. In the following, which of the named applications our created dataset could be particularly suitable for will be summarized. The first presented application referred to an increased knowledge on how regions of interest are dependent on the moisture sup-

ply from other regions. The provided dataset could provide valuable information to answer those questions but shows the following limitation: while the dataset includes comprehensive information on the fate of evaporation, information regarding the sources of precipitation is limited to land areas and cannot be displayed across the whole grid of land and sea cells. The reason for this is the chosen tracking direction (forward in time) and the focus on land grid cells for the tracking in order to reduce computational efforts. Nevertheless, the dataset quantifies the amount of precipitation originating

**Table 3.** Fate of evaporation and source of precipitation: examples for country tables.

Brazil Evaporation: 1240.2 mm a <sup>-1</sup> Precipitation: 1868.4 mm a <sup>-1</sup>				Egypt Evaporation: 104.0 mm a <sup>-1</sup> Precipitation: 13.1 mm a <sup>-1</sup>				Laos Evaporation: 1178.9 mm a <sup>-1</sup> Precipitation: 2176.9 mm a <sup>-1</sup>			
Fate of evaporation		Origin of precipitation		Fate of evaporation		Origin of precipitation		Fate of evaporation		Origin of precipitation	
Site	In %	Site	In %	Site	In %	Site	In %	Site	In %	Site	In %
Brazil	43.6	Sea	63.3	Sea	31.3	Sea	76.6	Sea	44.5	Sea	70.0
Sea	33.6	Brazil	28.9	Russia	7.3	Egypt	2.7	China	26.1	Thailand	6.4
Peru	4.7	Bolivia	1.2	China	5.6	Turkey	1.9	Laos	7.5	Laos	4.1
Colombia	4.5	Peru	0.6	India	5.0	Greece	1.2	Vietnam	5.0	India	3.9
Bolivia	4.3	Argentina	0.6	Ethiopia	4.7	Libya	1.1	Burma	4.2	Burma	3.6
Argentina	4.0	Angola	0.4	Iran	3.5	Sudan/South Sudan	0.9	Thailand	4.2	China	3.4
Paraguay	1.5	Paraguay	0.4	Sudan/South Sudan	3.5	Algeria	0.9	India	1.2	Vietnam	1.9
Ecuador	1.2	Venezuela	0.3	Turkey	3.4	Nigeria	0.8	Russia	1.1	Cambodia	1.3
Venezuela	0.8	Guyana	0.3	Kazakhstan	2.3	United States	0.8	Indonesia	0.9	Indonesia	0.4
Uruguay	0.6	Colombia	0.3	DR Congo	2.2	Italy	0.8	Cambodia	0.8	Russia	0.3

from the sea without knowing the exact non-terrestrial source locations. Examples for this were given in Table 3.

The second presented application was related to predictions of potential impacts of human-induced land cover changes on the water cycle. The created dataset could serve as an estimate for the question how land cover changes and altered amounts of land evaporation would potentially affect the supply of water via reprecipitation elsewhere (Keys et al., 2012). Van der Ent et al. (2010) stated within this context that decreasing evaporation (e.g., via deforestation) for areas with high shares of moisture recycling over land “would enhance droughts in downwind areas where overall precipitation amounts are low”. The opposing statement to that would also be conceivable – namely that increased land evaporation in these areas could also result in positive water supply effects. Such first-order estimates are relevant in the context of socio-hydrology (Keys and Wang-Erlandsson, 2018; Sivapalan et al., 2012), but we highlight at this point that the dataset can generally not provide more than rough estimates regarding this topic. An exception could be the inspection of interannual data for sites where major land cover changes occurred within the covered time period. However, for more comprehensive information on this subject it is advised to apply atmospheric moisture tracking directly to different land cover scenarios.

With regard to the third stated application, sustainability studies and water footprinting, the provided dataset also shows promising usage possibilities. Knowledge of the fate of evaporation was firstly integrated within the method of water footprinting by Berger et al. (2014, 2018) via an enhanced water accounting method. This considered atmospheric moisture recycling ratios within drainage basins, which could reduce water consumption patterns significantly (Berger et al., 2014, 2018). Aspects of moisture recycling across basin boundaries have not yet been considered. Comprehensive information about the fate of land evaporation in the dataset could be used for research regarding this topic.

The fourth possible application was related to research on the variability of precipitation and included seasonal and interannual variabilities. As the dataset provides both monthly data averaged over the considered time period and interannual data, it shows a high suitability for this kind of usage. Limitations with regard to the usage of seasonal data could be related to possible mismatches in the water balance, which should be verified before usage. However, for the yearly averages those mismatches become negligibly small. The application of studying interannual variability, on the other hand, is limited to the covered time period (years 2001 to 2018).

Precipitation changes and trends represented the fifth application focus. The dataset can be used in this context to understand changes and trends of moisture recycling for the considered time period, whereas predictions into the future are not possible. The sixth and seventh application were related to impacts of climate change on the hydrological cycle and the understanding of extreme weather events. The usage of the dataset for the determination of impacts related to climate change is limited to changes in climate which are reflected by the reanalysis data considered for this study. However, for a deeper analysis of the relationship between global temperature increases and resulting changes in moisture supply patterns, models including scenario analyses would be more suitable. With regard to the understanding of extreme weather events, the dataset could be used in order to gain an increased knowledge of the causes for past droughts. This could be achieved via investigations into anomalies of moisture supply patterns for relevant locations and time periods covered by the model. Investigations into extreme weather events such as floods, on the other hand, are not possible with this dataset as those would require a modeling with higher spatial and temporal resolutions.

## 4.2 Critical reflections on the used input data

The following section deals with the critical reflection on the ERA-I data (Berrisford et al., 2011; Dee et al., 2011), which were used as input for the creation of the dataset. ERA-I, which has been updated during the process of the preparation of this article to ERA5 (Hersbach et al., 2020), “showed both a comparatively reasonable closure of the terrestrial and atmospheric water balance as well as a reasonable agreement with observation datasets” (Lorenz and Kunstmann, 2012). It has been frequently used to study the hydrological cycle (Li et al., 2019) and ranks among the best representations of the hydrological processes within the atmosphere (Gao et al., 2014; Lorenz and Kunstmann, 2012). However, within the past some biases were also reported, especially with regard to the variables of evaporation and precipitation (Bumke, 2016; Fu et al., 2016). Plots for these two variables are presented as daily averages in Fig. S37 of the Supplement. Moreover, we provide a grid-cell-based comparison between ERA-I and its successor version ERA5 in Fig. S38 of the Supplement. This revealed that the variations in evaporation (Fig. S38, part a) and precipitation (Fig. S38, part b) between the two data sources are relatively small in most regions ( $\ll 1$  mm). The differences in precipitation (Fig. S38, part b), however, can also take higher values of up to 2, 3 or even more than 4 mm d<sup>-1</sup> for a few connected regions. Those can mainly be found within the high-precipitation areas of the tropics and along the western coast of North and South America. Considering that ERA5 claims in particular an improved performance over land in the deep tropics (ECMWF, 2020; Hersbach et al., 2020), precipitation in ERA-I might be slightly overestimated (e.g., in Central Africa) or underestimated (e.g., on Borneo) for some of the tropical regions.

Next to the grid-cell-based comparison of ERA-I to ERA5, we provide an additional analysis on continental scales. This compares the average continental evaporation and precipitation of ERA-I to ERA5 and a study by Rodell et al. (2015). The latter combined a variety of data sources, such as GPCP v2.2 (Adler et al., 2003), SeaFlux v1.0 (Clayson et al., 2012), MERRA (Bosilovich et al., 2011), MERRA-Land (Reichle, 2012) and GLDAS (Rodell et al., 2004), to derive an observed state of the water cycle in the early 21st century. Methodological details regarding the comparison can be reviewed in the Supplement. Table 4 presents the derived results, which cover all continents except Antarctica plus the overall global land, global ocean and the Earth as a whole. We stress that a final conclusion on which dataset is closest to reality is regarded as out of the scope of this paper. We can, however, conclude that repeating our analysis with ERA5 would overall not lead to major differences. This is due to the fact that both the continental comparison (Table 4) and the grid-cell-based comparison (Fig. S38) between ERA-I and ERA5 revealed generally high similarities for most regions. The comparison to Rodell et al. (2015), on the other hand, led to more significant differences. Table 4 demonstrates that the

**Table 4.** Continental evaporation ( $E$ ) and precipitation ( $P$ ) of ERA-I (Berrisford et al., 2011; Dee et al., 2011) in comparison to ERA5 (Hersbach et al., 2020) and the study by Rodell et al. (2015).

Regions	Evaporation in mm d <sup>-1</sup>			$\Delta$ in %		Precipitation in mm d <sup>-1</sup>			$\Delta$ in %	
	ERA-I	ERA5	Rodell et al. (2015)	ERA-I to ERA5	ERA-I to Rodell et al. (2015)	ERA-I	ERA5	Rodell et al. (2015)	ERA-I to ERA5	ERA-I to Rodell et al. (2015)
North America	1.34	1.49	1.13	-10.1%	+18.6%	1.95	2.20	2.02	-11.4%	-3.5%
South America	3.00	2.97	2.67	+1.0%	+12.4%	4.96	5.40	4.57	-8.1%	+8.5%
Eurasia	1.41	1.40	1.16	+0.7%	+21.6%	2.09	2.18	1.98	-4.1%	+5.6%
Africa	1.76	1.75	1.54	+0.6%	+14.3%	2.13	1.92	1.89	+10.9%	+12.7%
Oceania	3.19	3.11	3.10	+2.6%	+2.9%	7.91	7.68	6.79	+3.0%	+16.5%
Australia	1.42	1.41	0.93	+0.7%	+52.7%	1.03	1.10	1.42	-6.4%	-27.5%
World land	1.59	1.61	1.32	-1.2%	+20.5%	2.31	2.40	2.18	-3.8%	+6.0%
World ocean	3.50	3.60	3.37	-2.8%	+3.9%	3.16	3.31	3.03	-4.5%	+4.3%
World	2.96	2.96	2.79	$\pm 0\%$	+6.1%	2.91	3.05	2.79	-4.6%	+4.3%

intensity of evaporation over land in both ERA-I and ERA5 seems overestimated compared to Rodell et al. (2015), especially in Australia (up to +52.7 %) and Eurasia (up to +21.6 %). A similar trend can be observed regarding the variable precipitation, where, except for North America and Australia, ERA-I and ERA5 show consistently higher values. With regard to precipitation over Australia, however, an opposing trend is visible. Here, ERA-I and ERA5 might underestimate precipitation over land, which would be in line with findings made by Fu et al. (2016) for this region.

Logically, at the end of this discussion, the question arises as to what users of the dataset could do if they find the ERA-I evaporation or precipitation data unreliable while, at the same time, more representative data is available. In this case, we recommend to solely use the relative source–receptor relationships of our dataset while plugging in their own data regarding the absolute values of evaporation and precipitation. This assumption will likely be satisfactory in cases where all data are equally biased, but when only certain areas are considered biased a correction procedure would be more complicated.

#### 4.3 Comparison to other data sets

At this point, a general comparison of our dataset to the existing one referring to the Lagrangian 3D quasi-isentropic back-trajectory (3D QIBT) method (DeSole and Dirmeyer, 2012; Dirmeyer et al., 2009) forced with the NCEP-DOE AMIP-II reanalysis (R-2) (Kanamitsu et al., 2002) and CMAP data (Xie and Arkin, 1997) is given. Next to a slightly higher spatial resolution (1.5° compared to 1.9° resolution), the results of our study are easier to access due to the publication of raw data and aggregated data in a public repository (ready-to-download data). An advantage of the dataset based on the 3D QIBT method, on the other hand, is a longer considered time period (25 to 18 years). A significant difference lies in the tracking direction of the two approaches. The 3D QIBT approach generally traces moisture backward in time, and its application led to comprehensive information on the sources of precipitation. By contrast, our study focus was on analyzing the fate of evaporation, which was realized through a forward tracking of atmospheric moisture. The different tracking directions led to different opportunities for the plotting of atmospheric watersheds. Our dataset enables the plotting of evaporationsheds over the whole considered grid of land and sea cells, whereas the plotting of precipitationsheds is limited to the areas of land. Vice versa, the dataset based on the QIBT method enables the plotting of precipitationsheds over the whole considered grid, whereas the plotting of evaporationsheds is limited to land cells. In order to exemplify differences of the study outputs, study results on a country level from Dirmeyer et al. (2009) were compared to the results of our dataset based on the following two data items:

- terrestrial evaporative source (TES is the fraction of precipitation that originated as evaporation from terrestrial sources) according to Dirmeyer et al. (2009),
- country-internal evaporative source (CIES is the fraction of precipitation that originated as evaporation from the same country), which is termed recycling ratio (RR) in Dirmeyer et al. (2009).

Tables 5 and 6 analyze the top 10 countries with the highest and lowest average TES and CIES values for both datasets. As a general trend, our dataset shows in most cases a higher ocean contribution for the evaporative sources of precipitation (derived by in general lower TES values). The main reason for this is probably that the data used by Dirmeyer et al. (2009) show a land evaporation that on average almost equals the precipitation over land (ratio of land evaporation to land precipitation: 0.99) and thus allow hardly any runoff (Trenberth et al., 2011; Xie and Arkin, 1997). This fact leads inevitably to TES values (as well as CIES values) that could be classified as being more on the high side. Moreover, there may be several methodological differences causing different outputs, such as different (vertical) mixing assumptions.

Next to general trends, different country compositions can be observed within the lists of the two datasets. Table 5 highlights that only 3 out of the 10 countries appear for both datasets within the list of the 10 highest TES values (Mongolia, the Central African Republic and Paraguay). In this context, in each case Mongolia represents the country with the highest share of precipitation originating from terrestrial sources (80.3 % – WAM-2layers and 95.7 % – 3D QIBT). Regarding the countries with the lowest TES values, both approaches list five countries in common (Chile, New Zealand, the Philippines, French Guiana and Portugal) while showing the lowest value for Chile (4.3 % – WAM-2layers and 8.1 % – 3D QIBT). Regarding the CIES (Table 6), high values appear in general for relatively large countries. At this point, 7 out of 10 countries are listed for both datasets within the top 10 (Brazil, Russia, China, DR Congo, Australia, United States and India). The highest value refers to Brazil (28.9 %) for the WAM-2layers method and to Russia (64.7 %) for the 3D QIBT approach. Small CIES values, on the other hand, appear for relatively small countries. Here we find five countries in common (Luxembourg, Qatar, Gambia, Israel and Djibouti), with Luxembourg showing the lowest value in each case (0.2 % – WAM-2layers and 0.4 % – 3D QIBT). The fact that different countries appear in the tables is most likely caused by spatial differences of evaporation, precipitation and wind speed in the underlying reanalysis input data. Differences regarding the tracking method itself, on the other hand, might play a less important role, as WAM-2layers was found to reach generally similar results to Lagrangian models (Van der Ent et al., 2013; Van der Ent and Tuinenburg, 2017). The overall comparison of the results for the TES and the CIES between the two methods including all countries can be gained from the Supplement (Table S2).

**Table 5.** Comparison of the top 10 countries with the highest and lowest average TES values between our dataset based on the WAM-2layers method and the one referring to the 3D QIBT method (Dirmeyer et al., 2009). Countries appearing in both lists are displayed in bold font (CAR stands for Central African Republic).

Rank	Top 10 countries with the highest TES				Top 10 countries with the lowest TES			
	WAM-2layers	in %	3D QIBT	in %	WAM-2layers	in %	3D QIBT	in %
1	<b>Mongolia</b>	80.3	<b>Mongolia</b>	95.7	<b>Chile</b>	4.3	<b>Chile</b>	8.1
2	Niger	72.0	<b>Paraguay</b>	90.0	<b>New Zealand</b>	8.8	<b>Portugal</b>	9.9
3	Chad	68.0	Nepal	85.5	<b>Philippines</b>	9.3	<b>New Zealand</b>	9.9
4	Mali	66.8	Namibia	84.2	<b>French Guiana</b>	12.0	Ireland	11.1
5	Cameroon	64.0	Bhutan	84.0	Papua New Guinea	12.2	<b>Philippines</b>	11.6
6	Burkina Faso	63.0	Russia	83.2	<b>Portugal</b>	12.4	Morocco	12.7
7	Mauritania	62.8	Botswana	82.9	Sri Lanka	13.1	Israel	13.3
8	<b>CAR</b>	62.1	Bolivia	82.7	Somalia	14.5	Lebanon	13.7
9	<b>Paraguay</b>	61.9	<b>CAR</b>	82.0	Suriname	14.8	<b>French Guiana</b>	14.5
10	Kyrgyzstan	60.9	Angola	81.3	Belize	15.5	United Kingdom	14.9

**Table 6.** Comparison of the top 10 countries with the highest and lowest average CIES values between our dataset based on the WAM-2layers method and the one referring to the 3D QIBT method (Dirmeyer et al., 2009). Countries appearing in both lists are displayed in bold font.

Rank	Top 10 countries with the highest CIES				Top 10 countries with the lowest CIES			
	WAM-2layers	in %	3D QIBT	in %	WAM-2layers	in %	3D QIBT	in %
1	<b>Brazil</b>	28.9	<b>Russia</b>	64.7	<b>Luxembourg</b>	0.2	<b>Luxembourg</b>	0.4
2	<b>Russia</b>	27.8	Canada	54.8	<b>Qatar</b>	0.3	<b>Qatar</b>	0.4
3	<b>China</b>	25.9	<b>Brazil</b>	46.3	Lebanon	0.5	Belize	0.5
4	<b>DR Congo</b>	25.1	<b>United States</b>	43.2	<b>Gambia</b>	0.8	<b>Gambia</b>	0.7
5	Angola	20.9	<b>China</b>	41.4	<b>Israel</b>	0.8	<b>Israel</b>	0.8
6	<b>Australia</b>	20.7	<b>Australia</b>	37.9	Western Sahara	0.9	Equatorial Guinea	1.2
7	Argentina	19.0	<b>India</b>	36.4	Jordan	0.9	<b>Djibouti</b>	1.3
8	<b>United States</b>	18.3	Mongolia	30.8	<b>Djibouti</b>	0.9	El Salvador	1.4
9	<b>India</b>	18.1	<b>DR Congo</b>	28.5	Belgium	1.0	Macedonia	1.4
10	Sudan/South Sudan	17.4	Mexico	28.4	Iceland	1.0	Rwanda	1.4

Larger overlaps between the two datasets could partly be identified while focusing on the top contributors for precipitation over individual countries. This is exemplified through Tables S3 to S5 of the Supplement, which provide an overview of the top 10 sources of precipitation for the sample countries Brazil, Egypt and Laos with regard to both datasets. The country of Laos in particular shows a relatively high match regarding the appearance of sources and their ranking to each other in this context. A more detailed direct interpretation of the differences in the results between individual countries is at this point regarded as out of scope for this paper but could be tackled by comparative studies in the future.

## 5 Data availability

The dataset on the fate of land evaporation is available within the PANGAEA research data repository. It can be accessed through <https://doi.org/10.1594/PANGAEA.908705> and cited as Link et al. (2019a). The dataset consists of

two sub-datasets – a basic dataset that contains data averaged over the whole considered time period and an interannual dataset providing data for separate years. An attached PDF file (“readme.pdf”) explains the structure of the dataset and gives all necessary information on how to work with it. In addition to the provided dataset, a screening tool for the visualization of evaporationsheds on a land grid cell to grid cell basis (based on matrix type 1 of Table 2) can be accessed through <http://wf-tools.see.tu-berlin.de/wf-tools/evaporationshed/#/> (Link et al., 2019b).

## 6 Conclusions

The background of this research was an increased occurrence of studies on the fate and origin of atmospheric moisture. Numerical moisture tracking has been highlighted as one of the main methods to study those aspects. To our knowledge, so far only one approach had been published that tried to track atmospheric moisture globally over a fine-meshed grid (Dirmeyer et al., 2009). This aimed mainly to determine the

sources of land precipitation (Dirmeyer et al., 2009). The goal of our study was the provision of a complementary publicly available high-resolution global dataset on the fate of land evaporation and was achieved via a global application of the numerical moisture tracking model WAM-2layers. Further post-processing resulted in monthly and yearly source–receptor matrices for average moisture transfers from land grid cells, countries and basins. Furthermore, raw data for interannual differences were compiled. The created dataset is the first publicly available ready-to-download dataset providing the overall shape of evaporationsheds for land cells of a global fine-meshed grid at a monthly resolution. Additionally, information on precipitationsheds can be gained via the dataset. The dataset can be regarded as a useful complement to the existing dataset referring to the QIBT method (Dirmeyer et al., 2009; DelSole and Dirmeyer, 2012). It is expected that it will facilitate the access to data on atmospheric moisture recycling and could be integrated into future studies. Possible applications were identified and refer mainly to studies on atmospheric moisture dependencies, impacts of land use changes, water footprinting, seasonal and interannual variabilities of precipitation, precipitation changes and trends, and droughts.

**Supplement.** The supplement related to this article is available online at: <https://doi.org/10.5194/essd-12-1897-2020-supplement>.

**Author contributions.** AL and RE adapted and tested the Python code. Furthermore, they conducted the main model run and the post-processing. AL, RE, and MB were responsible for the results presentation, the plausibility checks, the interpretation of the results, and the compilation of the dataset. AL, RE, MB, and MF worked on the preparation of the manuscript. SE provided the basin mask from the WaterGAP3 model and gave advisory support for the post-processing in ArcGIS.

**Competing interests.** The authors declare that they have no conflict of interest.

**Acknowledgements.** The authors acknowledge the HLRN for providing high-performance computing resources that have contributed to the research results reported in this paper. In particular, the support of Wolfgang Baumann from the HLRN concerning technical and implementation aspects in making the code run on those resources is gratefully acknowledged.

**Financial support.** This research has been supported by the Deutsche Forschungsgemeinschaft (project no. FI 1622/4-1) and the Netherlands Organization for Scientific Research (project no. 016.Veni.181.015).

**Review statement.** This paper was edited by Scott Stevens and reviewed by three anonymous referees.

## References

- Adler, R. F., Huffman, G. J., Chang, A., Ferraro, R., Xie, P. P., Janowiak, J., Rudolf, B., Schneider, U., Curtis, S., Bolvin, D., Gruber, A., Susskind, J., Arkin, P., and Nelkin, E.: The version-2 global precipitation climatology project (GPCP) monthly precipitation analysis (1979–present), *J. Hydrometeorol.*, 4, 1147–1167, [https://doi.org/10.1175/1525-7541\(2003\)004<1147:TVGPCP>2.0.CO;2](https://doi.org/10.1175/1525-7541(2003)004<1147:TVGPCP>2.0.CO;2), 2003.
- Bagley, J. E., Desai, A. R., Dirmeyer, P. A., and Foley, J. A.: Effects of land cover change on moisture availability and potential crop yield in the worlds breadbaskets, *Environ. Res. Lett.*, 7, 014009, <https://doi.org/10.1088/1748-9326/7/1/014009>, 2012.
- Berger, M., Van der Ent, R., Eisner, S., Bach, V., and Finkbeiner, M.: Water accounting and vulnerability evaluation (WAVE): Considering atmospheric evaporation recycling and the risk of freshwater depletion in water footprinting, *Environ. Sci. Technol.*, 48, 4521–4528, <https://doi.org/10.1021/es404994t>, 2014.
- Berger, M., Eisner, S., Van der Ent, R., Flörke, M., Link, A., Poligkei, J., Bach, V., and Finkbeiner, M.: Enhancing the Water Accounting and Vulnerability Evaluation Model: WAVE+, *Environ. Sci. Technol.*, 52, 10757–10766, <https://doi.org/10.1021/acs.est.7b05164>, 2018.
- Berrisford, P., Dee, D. P., Poli, P., Brugge, R., Fielding, K., Fuentes, M., Källberg, P., Kobayashi, S., Uppala, S., and Simmons, A.: The ERA-Interim archive Version 2.0. ERA Report Series 1, available at: <http://www.ecmwf.int/en/eLibrary/8174-era-interim-archive-version-20> (last access: 27 September 2019), 2011.
- Bosilovich, M. G., Schubert, S. D., and Walker, G. K.: Global changes of the water cycle intensity, *J. Climate*, 18, 1591–1608, <https://doi.org/10.1175/JCLI3357.1>, 2005.
- Bosilovich, M. G., Robertson, F. R., and Chen, J.: Global energy and water budgets in MERRA, *J. Climate*, 24, 5721–5739, <https://doi.org/10.1175/2011JCLI4175.1>, 2011.
- Bumke, K.: Validation of ERA-interim precipitation estimates over the baltic sea, *Atmosphere-Basel*, 7, 82, <https://doi.org/10.3390/atmos7060082>, 2016.
- Clayson, C. A., Roberts, J. B., and Bogdanoff, A. S.: The SeaFlux Turbulent Flux Dataset The SeaFlux Turbulent Flux Dataset Version 1 0 Documentation The SeaFlux Turbulent Flux Dataset, available at: <https://ntrs.nasa.gov/archive/nasa/casi.ntrs.nasa.gov/20120004203.pdf> (last access: 21 August 2020), 2012.
- Cun, J. L.: Global country boundaries, available at: <https://www.arcgis.com/home/item.html?id=2ca75003ef9d477fb22db19832c9554f> (last access: 27 September 2019), 2016.
- Dee, D. P., Uppala, S. M., Simmons, A. J., Berrisford, P., Poli, P., Kobayashi, S., Andrae, U., Balmaseda, M. A., Balsamo, G., Bauer, P., Bechtold, P., Beljaars, A. C. M., van de Berg, L., Bidlot, J., Bormann, N., Delsol, C., Dragani, R., Fuentes, M., Geer, A. J., Haimberger, L., Healy, S. B., Hersbach, H., Hólm, E. V., Isaksen, L., Källberg, P., Köhler, M., Matricardi, M., McNally, A. P., Monge-Sanz, B. M., Morcrette, J. J., Park, B. K., Peubey, C., de Rosnay, P., Tavolato, C., Thépaut, J. N., and Vitart, F.: The

- ERA-Interim reanalysis: Configuration and performance of the data assimilation system, *Q. J. Roy. Meteor. Soc.*, 137, 553–597, <https://doi.org/10.1002/qj.828>, 2011.
- DelSole, T. M. and Dirmeyer, P. A.: Characterizing Land Surface Memory to Advance Climate Prediction, available at: <http://cola.gmu.edu/wcr/> (last access: 27 September 2019), 2012.
- Dirmeyer, P. A. and Brubaker, K. L.: Contrasting evaporative moisture sources during the drought of 1988 and the flood of 1993, *J. Geophys. Res.-Atmos.*, 104, 19383–19397, <https://doi.org/10.1029/1999JD900222>, 1999.
- Dirmeyer, P. A., Brubaker, K. L., and DelSole, T.: Import and export of atmospheric water vapor between nations, *J. Hydrol.*, 365, 11–22, <https://doi.org/10.1016/j.jhydrol.2008.11.016>, 2009.
- Dominguez, F., Miguez-Macho, G., and Hu, H.: WRF with water vapor tracers: A study of moisture sources for the North American Monsoon, *J. Hydrometeorol.*, 17, 1915–1927, <https://doi.org/10.1175/JHM-D-15-0221.1>, 2016.
- Dominguez, F., Hu, H., and Martinez, J. A.: Two-Layer Dynamic Recycling Model (2L-DRM): Learning from Moisture Tracking Models of Different Complexity, *J. Hydrometeorol.*, 21, 3–16, <https://doi.org/10.1175/JHM-D-19-0101.1>, 2019.
- Drumond, A., Stojanovic, M., Nieto, R., Vicente-Serrano, S. M., and Gimeno, L.: Linking Anomalous Moisture Transport And Drought Episodes in the IPCC Reference Regions, *B. Am. Meteorol. Soc.*, 100, 1481–1498, <https://doi.org/10.1175/bams-d-18-0111.1>, 2019.
- ECMWF: What are the changes from ERA-Interim to ERA5?, available at: <https://confluence.ecmwf.int/pages/viewpage.action?pageId=74764925>, last access: 4 June 2020.
- Eisner, S.: Comprehensive Evaluation of the WaterGAP3 Model across Climatic, Physiographic, and Anthropogenic Gradients, PhD thesis, University of Kassel, Kassel, 128 pp., 2016.
- Findell, K. L., Keys, P. W., van der Ent, R. J., Lintner, B. R., Berg, A., and Krasting, J. P.: Rising Temperatures Increase Importance of Oceanic Evaporation as a Source for Continental Precipitation, *J. Climate*, 32, 7713–7726, <https://doi.org/10.1175/jcli-d-19-0145.1>, 2019.
- Fu, G., Charles, S. P., Timbal, B., Jovanovic, B., and Ouyang, F.: Comparison of NCEP-NCAR and ERA-Interim over Australia, *Int. J. Climatol.*, 36, 2345–2367, <https://doi.org/10.1002/joc.4499>, 2016.
- Gangoiti, G., Gómez-Domenech, I., De Cmara, E. S., Alonso, L., Navazo, M., Iza, J., García, J. A., Ilardia, J. L., and Millán, M. M.: Origin of the water vapor responsible for the European extreme rainfalls of August 2002: 2. A new methodology to evaluate evaporative moisture sources, applied to the August 11–13 central European rainfall episode, *J. Geophys. Res.-Atmos.*, 116, D21103, <https://doi.org/10.1029/2010JD015538>, 2011.
- Gao, Y., Cuo, L., and Zhang, Y.: Changes in moisture flux over the tibetan plateau during 1979–2011 and possible mechanisms, *J. Climate*, 27, 1876–1893, <https://doi.org/10.1175/JCLI-D-13-00321.1>, 2014.
- Gimeno, L., Stohl, A., Trigo, R. M., Dominguez, F., Yoshimura, K., Yu, L., Drumond, A., Durn-Quesada, A. M., and Nieto, R.: Oceanic and terrestrial sources of continental precipitation, *Rev. Geophys.*, 50, 1–41, <https://doi.org/10.1029/2012RG000389>, 2012.
- Gimeno, L., Dominguez, F., Nieto, R., Trigo, R., Drumond, A., Reason, C. J. C., Taschetto, A. S., Ramos, A. M., Kumar, R., and Marengo, J.: Major Mechanisms of Atmospheric Moisture Transport and Their Role in Extreme Precipitation Events, *Annu. Rev. Env. Resour.*, 41, 117–141, <https://doi.org/10.1146/annurev-environ-110615-085558>, 2016.
- Goessling, H. F. and Reick, C. H.: On the “well-mixed” assumption and numerical 2-D tracing of atmospheric moisture, *Atmos. Chem. Phys.*, 13, 5567–5585, <https://doi.org/10.5194/acp-13-5567-2013>, 2013.
- Guo, L., Van der Ent, R. J., Klingaman, N. P., Demory, M. E., Vidale, P. L., Turner, A. G., Stephan, C. C., and Chevuturi, A.: Moisture sources for East Asian precipitation: Mean seasonal cycle and interannual variability, *J. Hydrometeorol.*, 20, 657–672, <https://doi.org/10.1175/JHM-D-18-0188.1>, 2019.
- Herrera-Estrada, J. E., Martinez, J. A., Dominguez, F., Findell, K. L., Wood, E. F., and Sheffield, J.: Reduced Moisture Transport Linked to Drought Propagation Across North America, *Geophys. Res. Lett.*, 46, 5243–5253, <https://doi.org/10.1029/2019GL082475>, 2019.
- Hersbach, H., Bell, B., Berrisford, P., Hirahara, S., Horányi, A., Muñoz-Sabater, J., Nicolas, J., Peubey, C., Radu, R., Schepers, D., Simmons, A., Soci, C., Abdalla, S., Abellan, X., Balsamo, G., Bechtold, P., Biavati, G., Bidlot, J., Bonavita, M., de Chiara, G., Dahlgren, P., Dee, D., Diamantakis, M., Dragani, R., Flemming, J., Forbes, R., Fuentes, M., Geer, A., Haimberger, L., Healy, S., Hogan, R. J., Hólm, E., Janisková, M., Keeley, S., Laloyaux, P., Lopez, P., Lupu, C., Radnoti, G., de Rosnay, P., Rozum, I., Vamborg, F., Villaume, S., and Thépaut, J.-N.: The ERA5 Global Reanalysis, *Q. J. Roy. Meteor. Soc.*, 146, 1999–2049, <https://doi.org/10.1002/qj.3803>, 2020.
- International Organization for Standardization: ISO 14046: Environmental management – Water footprint – Principles, requirements and guidelines (German and English version EN ISO 14046:2016), Geneva, 2016.
- Kanamitsu, M., Ebisuzaki, W., Woollen, J., Yang, S. K., Hnilo, J. J., Fiorino, M., and Potter, G. L.: NCEP-DOE AMIP-II reanalysis (R-2), *B. Am. Meteorol. Soc.*, 83, 1631–1644, [https://doi.org/10.1175/bams-83-11-1631\(2002\)083<1631:nar>2.3.co;2](https://doi.org/10.1175/bams-83-11-1631(2002)083<1631:nar>2.3.co;2), 2002.
- Keune, J. and Miralles, D. G.: A precipitation recycling network to assess freshwater vulnerability: Challenging the watershed convention, *Water Resour. Res.*, 55, 9947–9961, <https://doi.org/10.1029/2019wr025310>, 2019.
- Keys, P. W. and Wang-Erlandsson, L.: On the social dynamics of moisture recycling, *Earth Syst. Dynam.*, 9, 829–847, <https://doi.org/10.5194/esd-9-829-2018>, 2018.
- Keys, P. W., van der Ent, R. J., Gordon, L. J., Hoff, H., Nikoli, R., and Savenije, H. H. G.: Analyzing precipitationsheds to understand the vulnerability of rainfall dependent regions, *Biogeosciences*, 9, 733–746, <https://doi.org/10.5194/bg-9-733-2012>, 2012.
- Keys, P. W., Wang-Erlandsson, L., and Gordon, L. J.: Megacity precipitationsheds reveal tele-connected water security challenges, *PLoS One*, 13, 1–22, <https://doi.org/10.1371/journal.pone.0194311>, 2018.
- Li, Y., Su, F., Chen, D., and Tang, Q.: Atmospheric Water Transport to the Endorheic Tibetan Plateau and Its Effect on the Hydrological Status in the Region, *J. Geophys. Res.-Atmos.*, 124, 12864–12881, <https://doi.org/10.1029/2019JD031297>, 2019.

- Link, A., Van der Ent, R., Berger, M., Eisner, S., and Finkbeiner, M.: The fate of land evaporation – A global dataset, PANGAEA, <https://doi.org/10.1594/PANGAEA.908705>, 2019a.
- Link, A., Van der Ent, R., Berger, M., Eisner, S., and Finkbeiner, M.: Tool for Visualizing the Fate of Land Evaporation, available at: <https://wf-tools.sea.tu-berlin.de/wf-tools/evaporationshed/#/> (last access: 16 December 2019), 2019b.
- Lorenz, C. and Kunstmann, H.: The hydrological cycle in three state-of-the-art reanalyses: Intercomparison and performance analysis, *J. Hydrometeorol.*, 13, 1397–1420, <https://doi.org/10.1175/JHM-D-11-088.1>, 2012.
- Miralles, D. G., Nieto, R., McDowell, N. G., Dorigo, W. A., Verhoest, N. E. C., Liu, Y. Y., Teuling, A. J., Dolman, A. J., Good, S. P., and Gimeno, L.: Contribution of water-limited ecoregions to their own supply of rainfall, *Environ. Res. Lett.*, 11, 1–12, <https://doi.org/10.1088/1748-9326/11/12/124007>, 2016.
- Nieto, R., Ciric, D., Vázquez, M., Liberato, M. L. R., and Gimeno, L.: Contribution of the main moisture sources to precipitation during extreme peak precipitation months, *Adv. Water Resour.*, 131, 103385, <https://doi.org/10.1016/j.advwatres.2019.103385>, 2019.
- Reichle, R.: The MERRA-Land Data Product – GMAO Office Note No. 3, available at: <https://gmao.gsfc.nasa.gov/pubs/docs/Reichle541.pdf> (last access: 21 August 2020), 2012.
- Rockström, J., Falkenmark, M., Karlberg, L., Hoff, H., Rost, S., and Gerten, D.: Future water availability for global food production: The potential of green water for increasing resilience to global change, *Water Resour. Res.*, 45, 1–16, <https://doi.org/10.1029/2007WR006767>, 2009.
- Rodell, M., Houser, P. R., Jambor, U., Gottschalck, J., Mitchell, K., Meng, C. J., Arsenault, K., Cosgrove, B., Radakovich, J., Bosilovich, M., Entin, J. K., Walker, J. P., Lohmann, D., and Toll, D.: The Global Land Data Assimilation System, *B. Am. Meteorol. Soc.*, 85, 381–394, <https://doi.org/10.1175/BAMS-85-3-381>, 2004.
- Rodell, M., Beaudoin, H. K., L’Ecuyer, T. S., Olson, W. S., Famiglietti, J. S., Houser, P. R., Adler, R., Bosilovich, M. G., Clayson, C. A., Chambers, D., Clark, E., Fetzer, E. J., Gao, X., Gu, G., Hilburn, K., Huffman, G. J., Lettenmaier, D. P., Liu, W. T., Robertson, F. R., Schlosser, C. A., Sheffield, J., and Wood, E. F.: The observed state of the water cycle in the early twenty-first century, *J. Climate*, 28, 8289–8318, <https://doi.org/10.1175/JCLI-D-14-00555.1>, 2015.
- Salih, A. A. M., Zhang, Q., Pausata, F. S. R., and Tjernström, M.: Sources of Sahelian-Sudan moisture: Insights from a moisture-tracing atmospheric model, *J. Geophys. Res.*, 121, 7819–7832, <https://doi.org/10.1002/2015JD024575>, 2016.
- Singh, H. K. A., Bitz, C. M., Donohoe, A., Nusbaumer, J., and Noone, D. C.: A mathematical framework for analysis of water tracers. Part II: Understanding large-scale perturbations in the hydrological cycle due to CO<sub>2</sub> doubling, *J. Climate*, 29, 6765–6782, <https://doi.org/10.1175/JCLI-D-16-0293.1>, 2016.
- Singh, H. K. A., Bitz, C. M., Donohoe, A., and Rasch, P. J.: A source-receptor perspective on the polar hydrologic cycle: Sources, seasonality, and arctic-antarctic parity in the hydrologic cycle response to CO<sub>2</sub> doubling, *J. Climate*, 30, 9999–10017, <https://doi.org/10.1175/JCLI-D-16-0917.1>, 2017.
- Sivapalan, M., Savenije, H. H. G., and Blöschl, G.: Socio-hydrology: A new science of people and water, *Hydrol. Process.*, 26, 1270–1276, <https://doi.org/10.1002/hyp.8426>, 2012.
- Sodemann, H., Schwierz, C., and Wernli, H.: Interannual variability of Greenland winter precipitation sources: Lagrangian moisture diagnostic and North Atlantic Oscillation influence, *J. Geophys. Res.-Atmos.*, 113, D03107, <https://doi.org/10.1029/2007JD008503>, 2008.
- Spracklen, D. V., Arnold, S. R., and Taylor, C. M.: Observations of increased tropical rainfall preceded by air passage over forests, *Nature*, 489, 282–285, <https://doi.org/10.1038/nature11390>, 2012.
- Staal, A., Tuinenburg, O. A., Bosmans, J. H. C., Holmgren, M., Van Nes, E. H., Scheffer, M., Zemp, D. C., and Dekker, S. C.: Forest-rainfall cascades buffer against drought across the Amazon, *Nat. Clim. Change*, 8, 539–543, <https://doi.org/10.1038/s41558-018-0177-y>, 2018.
- Trenberth, K. E., Fasullo, J. T., and Mackaro, J.: Atmospheric moisture transports from ocean to land and global energy flows in reanalyses, *J. Climate*, 24, 4907–4924, <https://doi.org/10.1175/2011JCLI4171.1>, 2011.
- Tuinenburg, O. A., Hutjes, R. W. A., and Kabat, P.: The fate of evaporated water from the Ganges basin, *J. Geophys. Res.-Atmos.*, 117, D01107, <https://doi.org/10.1029/2011JD016221>, 2012.
- Van der Ent, R. J.: A new view on the hydrological cycle over continents, PhD thesis, Delft University of Technology, Delft, 96 pp., 2014.
- Van der Ent, R. J.: WAM-2layers python, available at: <https://github.com/ruudvdent/WAM2layersPython> (last access: 24 March 2020), 2019.
- Van der Ent, R. J. and Savenije, H. H. G.: Oceanic sources of continental precipitation and the correlation with sea surface temperature, *Water Resour. Res.*, 49, 3993–4004, <https://doi.org/10.1002/wrcr.20296>, 2013.
- Van der Ent, R. J. and Tuinenburg, O. A.: The residence time of water in the atmosphere revisited, *Hydrol. Earth Syst. Sci.*, 21, 779–790, <https://doi.org/10.5194/hess-21-779-2017>, 2017.
- Van der Ent, R. J., Savenije, H. H. G., Schaeffli, B. and Steele-Dunne, S. C.: Origin and fate of atmospheric moisture over continents, *Water Resour. Res.*, 46, 1–12, <https://doi.org/10.1029/2010WR009127>, 2010.
- Van der Ent, R. J., Tuinenburg, O. A., Knoche, H.-R., Kunstmann, H., and Savenije, H. H. G.: Should we use a simple or complex model for moisture recycling and atmospheric moisture tracking?, *Hydrol. Earth Syst. Sci.*, 17, 4869–4884, <https://doi.org/10.5194/hess-17-4869-2013>, 2013.
- Van der Ent, R. J., Wang-Erlandsson, L., Keys, P. W., and Savenije, H. H. G.: Contrasting roles of interception and transpiration in the hydrological cycle – Part 2: Moisture recycling, *Earth Syst. Dynam.*, 5, 471–489, <https://doi.org/10.5194/esd-5-471-2014>, 2014.
- Wang-Erlandsson, L., Fetzer, I., Keys, P. W., van der Ent, R. J., Savenije, H. H. G., and Gordon, L. J.: Remote land use impacts on river flows through atmospheric teleconnections, *Hydrol. Earth Syst. Sci.*, 22, 4311–4328, <https://doi.org/10.5194/hess-22-4311-2018>, 2018.
- Wei, J., Dirmeyer, P. A., Wisser, D., Bosilovich, M. G., and Mocko, D. M.: Where does the irrigation water go? An estimate of the contribution of irrigation to precipitation using MERRA, *J. Hy-*



- drometeorol., 14, 275–289, <https://doi.org/10.1175/JHM-D-12-079.1>, 2013.
- Wei, J., Knoche, H. R., and Kunstmann, H.: Atmospheric residence times from transpiration and evaporation to precipitation: An age-weighted regional evaporation tagging approach, *J. Geophys. Res.*, 121, 6841–6862, <https://doi.org/10.1002/2015JD024650>, 2016.
- Xie, P. and Arkin, P. A.: Global Precipitation: A 17-Year Monthly Analysis Based on Gauge Observations, Satellite Estimates, and Numerical Model Outputs, *B. Am. Meteorol. Soc.*, 78, 2539–2558, [https://doi.org/10.1175/1520-0477\(1997\)078<2539:GPAYMA>2.0.CO;2](https://doi.org/10.1175/1520-0477(1997)078<2539:GPAYMA>2.0.CO;2), 1997.
- Zemp, D. C., Schleussner, C. F., Barbosa, H. M. J., Hirota, M., Montade, V., Sampaio, G., Staal, A., Wang-Erlandsson, L., and Rammig, A.: Self-amplified Amazon forest loss due to vegetation-atmosphere feedbacks, *Nat. Commun.*, 8, 1–10, <https://doi.org/10.1038/ncomms14681>, 2017.
- Zhang, C., Tang, Q., and Chen, D.: Recent changes in the moisture source of precipitation over the tibetan plateau, *J. Climate*, 30, 1807–1819, <https://doi.org/10.1175/JCLI-D-16-0493.1>, 2017.
- Zhang, C., Tang, Q., Chen, D., Van der Ent, R. J., Liu, X., Li, W., and Haile, G. G.: Moisture source changes contributed to different precipitation changes over the northern and southern Tibetan Plateau, *J. Hydrometeorol.*, 20, 217–229, <https://doi.org/10.1175/JHM-D-18-0094.1>, 2019.
- Zhao, L., Liu, X., Wang, N., Kong, Y., Song, Y., He, Z., Liu, Q., and Wang, L.: Contribution of recycled moisture to local precipitation in the inland Heihe River Basin, *Agr. Forest Meteorol.*, 271, 316–335, <https://doi.org/10.1016/j.agrformet.2019.03.014>, 2019.
- Zhao, T., Zhao, J., Hu, H., and Ni, G.: Source of atmospheric moisture and precipitation over China's major river basins, *Front. Earth Sci.*, 10, 159–170, <https://doi.org/10.1007/s11707-015-0497-4>, 2016.